MATERIALS SCIENCE

Rapid self-assembly of robust ultrathin ionogel films for high-performance bioelectronics

Na Li[1], Ping He[2], Zhihui Qin[1,3]*, Yichen Yan[2], Sidi Duan[2], Yunfeng Li[1], Xiaojiao Shi[1], Yuxuan Qiao[1], Junan Jiang[3], Tifeng Jiao[1]*, Ximin He[2]*

Ionogels, polymer networks infiltrated with ionic liquids (ILs), are promising for flexible electronics but face trade-offs among mechanical robustness, ultrathin form factors, and scalable fabrication. We present an IL-induced self-assembly strategy enabling the rapid formation of ultrathin polyvinyl alcohol (PVA) ionogel films. Upon contact with ILs, PVA chains spontaneously organize into a robust, noncovalently cross-linked network, achieving ultrafast conversion (<5 s) of viscous precursors into films with tunable thickness (13 to 103 μm). The resulting ionogel films combine high tensile strength (9.69 MPa), toughness (35.93 MJ m^{-3}), good ionic conductivity (0.2 S m^{-1}), and excellent environmental stability. This approach allows in situ formation of conformal ionogel coatings on complex, nonplanar surfaces, yielding seamless skin-device interfaces that retain stable functionality under repetitive deformation. Ionogel-based bioelectrodes capture diverse electrophysiological signals with high fidelity while serving as stretchable substrates for printed circuits and electrode arrays. Compatibility with diverse ILs highlights the versatility of this rapid, scalable approach for fabricating ultrathin ionogels with broadly tunable properties.

INTRODUCTION

Stretchable electronics, which can maintain stable performance under mechanical deformation, have emerged as promising candidates for next-generation on-skin devices (*1*), human-machine interfaces (*2*), and soft robotics (*3*). In these applications, stretchable devices are usually integrated onto complex, nonplanar surfaces, such as the human skin. Therefore, establishing a conformal and mechanically robust interface is essential to ensure high fidelity and stable signal acquisition at target sites (*4*). In addition, high mechanical toughness is required to maintain reliable performance under repeated or severe deformation due to dynamic mechanical stresses (*5*). Furthermore, for tissue-integrated bioelectronics, good conductivity is desirable to facilitate effective coupling between ionic fluxes in biological tissues and electronic current in stretchable electronics (*6*). Early studies have explored flexible electronic devices fabricated from various stretchable polymer films, such as polydimethylsiloxane (PDMS) (*7*), polyimide (PI) (*8*), polyethylene terephthalate (*9*), and Ecoflex (*10*). To enhance conformal contact with nonplanar surfaces, substrate thickness is often reduced to produce ultrathin flexible electronics (*11*, *12*). However, reducing thickness typically compromises the mechanical robustness of stretchable substrates, and the lack of adhesion further impede stable integration on nonplanar surfaces, resulting in detachment during repetitive deformations (*12*). Furthermore, the nonporous architecture of these polymer films restricts gas permeability, potentially causing adverse skin reactions, including allergies and inflammation (*13*). Most critically, for on-skin bioelectronics, the intrinsically low electrical transport and limited conformability of these polymer films weaken the capacitive coupling at the skin-device interface, producing a high-impedance interface that degrades both signal fidelity and overall device performance (*14*).

Ionically conductive gels, including hydrogels and ionogels, comprising crosslinked polymer networks solvated with mobile ions, have been extensively used in flexible and stretchable electronics due to their porous architecture, biomimetic ionic conductivity, mechanical compliance, and tunable adhesive properties (*15*, *16*). Ultrathin hydrogels with skin adhesion and mechanical softness can minimize interfacial gaps and conform intimately to textured skin surfaces (*17*–*19*). However, their intrinsic tendency to dehydrate under ambient conditions severely limits their long-term application in stretchable electronics. Compared to hydrogels, ionogels are regarded as more promising candidates for stretchable electronics with higher mechanical compliance and superior environmental stability (*20*). Recent advances have produced ionogels with high mechanical strength, good conductivity, and strong adhesion (*9*, *21*, *22*). Nevertheless, critical challenges remains when ionogels are used in flexible electronic devices. First, although emerging fabrication strategies have enabled the production of ultrathin ionogels, a fundamental trade-off persists between mechanical robustness and film thickness (*23*–*25*). These ultrathin ionogels often suffer from compromised mechanical performance, primarily due to the weakening effect of ionic liquids (ILs) on polymer-polymer interactions and insufficient crosslinking within the ultrathin structure (*23*). Second, an inherent conflict exists between conformal adhesion and mechanical durability. Enhancing conformal adhesion by softening the ionogel matrix typically reduces mechanical robustness, lowering reliability under substantial stress or cyclic loading (*26*). Third, achieving high-performance properties while enabling rapid, scalable fabrication remains challenging. For example, high-strength ultrathin ionogels usually require multistep processes such as electrospinning, sequential crosslinking, or repeated freeze-thaw cycles, which require longer fabrication time, higher costs, and limited scalability (*25*). These laborious and time-consuming preparation processes severely hinder the widespread adoption of ultrathin ionogels in scenarios demanding rapid, scalable fabrication, and even in situ gelation to achieve reliable conformability on complex and nonplanar surfaces (*27*). Therefore, reconciling these conflicts and developing a rapid, scalable strategy to fabricate ultrathin ionogel films with both

[1]State Key Laboratory of Metastable Materials Science and Technology, Hebei Key Laboratory of Applied Chemistry, Yanshan University, Qinhuangdao 066004, China. [2]Department of Materials Science and Engineering, University of California, Los Angeles, CA 90095, USA. [3]Department of Chemical and Biomolecular Engineering, National University of Singapore, 4 Engineering Drive 4, Singapore 117585, Singapore.
*Corresponding author. Email: zhqin@ysu.edu.cn (Z.Q.); tfjiao@ysu.edu.cn (T.J.); ximinhe@ucla.edu (X.H.)

high mechanical robustness and excellent conformability remains a pressing challenge.

Here, we report a rapid and scalable strategy for fabricating ultrathin ionogel films via an IL-induced self-assembly mechanism (Fig. 1A). Introducing IL into a high-viscosity polyvinyl alcohol (PVA) aqueous solution triggers spontaneous hierarchical aggregation and self-assembly of PVA chains, forming a dense, noncovalently cross-linked network. This enables ultrafast gelation within 5 s and scalable conversion of thick precursor layers into ultrathin ionogels with strong mechanical performance. This method also supports in situ formation of conformal, shape-adaptive coatings on complex, nonplanar surfaces, establishing seamless and stable interfaces owing to their ultrathin architecture and intrinsic adhesiveness. The resulting ionogel films, with tunable thicknesses from 13 to 103 μm, exhibit

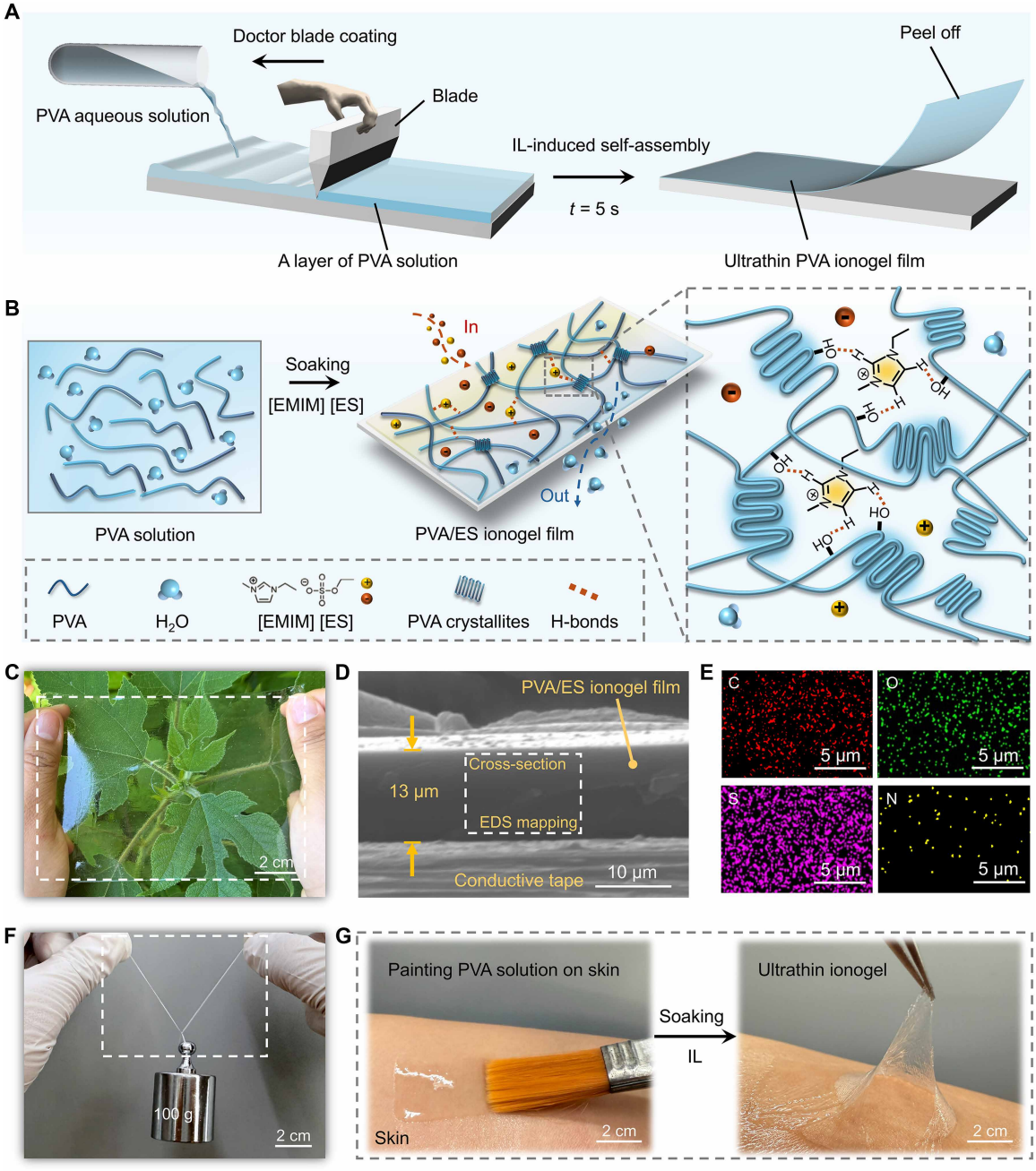

Fig. 1. Fabrication of highly robust and ultrathin ionogel films. (**A**) Schematic illustration of the rapid preparation process for ultrathin ionogel films via IL-induced self-assembly strategy. (**B**) Schematic diagrams depicting the formation mechanism and crosslinking structure of PVA/ES ionogel films. (**C**) Photograph of a large-sized PVA/ES ionogel film (10 cm by 13 cm). (**D** and **E**) Cross-sectional SEM image of the PVA/ES ionogel film (D) and corresponding EDS elemental mapping of the cross section (E). (**F**) Photograph of the PVA/ES ionogel film with a cross section of 10 mm by 13 μm holding up a 100-g weight. (**G**) Seamless, conformal adhesion of the PVA/ES ionogel film onto human skin via a painting-soaking fabrication process.

excellent tensile strength (9.69 MPa), toughness (35.93 MJ m^{-3}), good ionic conductivity (0.2 S m^{-1}), and outstanding environmental stability. We demonstrate direct fabrication of conformal and robust ultrathin ionogel-based bioelectrodes on wrinkled and hairy skin, enabling reliable, high-fidelity electrophysiological recordings. Furthermore, their suitability is shown as stretchable substrates by constructing flexible circuits and multichannel electrode arrays via three-dimensional (3D) printing. This versatile approach is compatible with various ILs, enabling tunable mechanical properties, and offers a powerful route for rapid, scalable fabrication of ultrathin, shape-adaptive ionogels for next-generation flexible and stretchable electronics.

RESULTS

Fabrication and formation process of PVA/ES ionogel films

PVA was selected as the polymeric framework owing to its simple molecular structure, abundant hydrogen bonding sites, excellent biocompatibility, and nontoxicity (*28*). To validate our IL-induced self-assembly strategy, 1-ethyl-3-methylimidazolium ethylsulfate ([EMIM] [ES])—a hydrophilic IL with high thermal stability, good conductivity, and biocompatibility (*22*)—was first used to construct PVA/ES ionogel films. Initially, PVA was dissolved in deionized water at elevated temperature to obtain PVA solution. Viscosity analysis of PVA solutions revealed that concentrations in the range of 16 to 24% (w/v) were suitable for preparing ionogel films (fig. S1). In particular, considering moderate viscosity for favorable coating uniformity, the 20% (w/v) PVA solution was selected as the optimal concentration (*29*). This solution was uniformly coated onto a glass substrate using the doctor blade coating (DBC) method and immediately immersed in an excess amount of [EMIM] [ES]. Within 5 s, [EMIM] [ES] quickly diffused into PVA solution layer, inducing the formation of a freestanding ionogel film that could be easily peeled from the glass substrate (fig. S2 and movie S1). As illustrated in Fig. 1B, [EMIM] [ES] played a dual role: (i) extracting water from the interchain regions of PVA, thereby promoting chain aggregation and the formation of noncovalent cross-linking sites (e.g., hydrogen bonds and PVA crystallites), and (ii) forming hydrogen bonds with PVA chains to further facilitate network assembly. This synergistic interaction enabled the ultrafast formation of ultrathin PVA/ES ionogels. The simple DBC-soaking process provided a rapid and scalable platform for producing ionogel films with tunable dimensions (movies S2 and S3). As shown in Fig. 1C, a transparent ionogel film measuring 10 cm by 13 cm was readily fabricated. Notably, this strategy allowed for the fabrication of ionogel films with tunable thicknesses (13 to 103 μm) by adjusting the blade-to-substrate gap and IL-induced self-assembly time (fig. S3 and table S1). Cross-sectional scanning electron microscopy (SEM) confirmed the formation of a 13-μm-thick PVA/ES ionogel film (Fig. 1D), while energy-dispersive spectroscopy (EDS) mapping revealed uniform distribution of elements C, O, N, and S along both perpendicular and parallel directions (Fig. 1E), confirming excellent compositional uniformity. A freestanding ionogel film could lift a 100-g weight (Fig. 1F), which was ~5880 times of its own weight, demonstrating excellent mechanical robustness. This method enabled the on-demand, in situ formation of adaptive, shape-conforming ionogel coatings on nonplanar surfaces within seconds (fig. S4). As demonstrated in Fig. 1G, the direct application of the PVA solution onto human skin followed by IL immersion rapidly yielded a conformal, ultrathin ionogel layer with intimate skin contact and robust interfacial adhesion.

To elucidate the formation mechanism, we investigated the IL-induced self-assembly behavior of PVA chains through a series of spectroscopic and structural characterizations. Raman spectra (Fig. 2A) showed that characteristic peaks of [EMIM] [ES] at 3166 and 3111 cm^{-1}, assigned to the HC-CH symmetric stretching and CH_3(N) HCH asymmetric stretching vibrations of the imidazole cation, shifted to 3160 and 3094 cm^{-1} in the PVA/ES ionogel film, respectively, indicating hydrogen bonding interactions between PVA hydroxyl groups and imidazole cation (*30*). In the pristine PVA solution, two distinct water-related peaks were observed at 3439 cm^{-1} (bound water with limited hydrogen bonding) and 3211 cm^{-1} (free water with tetrahedral hydrogen-bond networks) (*31*). Upon immersion in [EMIM] [ES], the intensity of the 3439 cm^{-1} peak markedly decreased, while the 3211 cm^{-1} peak disappeared entirely in the ionogel film. Deconvolution of the O—H stretching region (Fig. 2B) showed that the relative area of the 3439 cm^{-1} peak dropped from 68.39% in the PVA solution to 18.78% in the ionogel film, while the 3211 cm^{-1} band vanished, indicating substantial dehydration (*32*). Thermogravimetric analysis (TGA, Fig. 2C) confirmed that the ionogel film contained a low water content of 8.9 weight % (wt %) (*33*). These results indicate that [EMIM] [ES] can effectively disrupt the bonding of water with PVA chains and promote water expulsion, thereby facilitating the self-assembly of PVA chains. Fourier transform infrared (FTIR) spectra further corroborated these findings: the C—H stretching vibration of imidazolium ring in $[EMIM]^+$, originally located at 3151 and 3101 cm^{-1}, shifted to 3149 and 3122 cm^{-1} in the ionogel film, respectively (Fig. 2D), confirming hydrogen-bond formation between PVA chains and [EMIM] [ES] (*21*). Additional absorption bands at 1141 and 1094 cm^{-1}, corresponding to C—O stretching vibrations in hydrogen-bonded crystalline PVA, emerged in the ionogel film, suggesting IL-induced crystallite formation (*34*). X-ray diffraction (XRD) patterns revealed a diffraction peak at $2\theta = 19.6°$ in the ionogel film, corresponding to the (101) reflection of semicrystalline PVA, but with reduced intensity compared with the PVA film (Fig. 2E), indicating lower crystallinity (*35*, *36*). From small-angle x-ray scattering (SAXS) patterns (Fig. 2F and fig. S5), it can be estimated that the average distance between adjacent crystalline domains in the ionogel film was 8.6 nm, which was larger than that of the PVA film (7.3 nm) (*37*), implying that although [EMIM] [ES] promotes the formation of crystalline domain, it also yields a looser crystalline structure due to IL-polymer interactions.

Based on the above results, we propose the following mechanism: Water is a relatively poor solvent for PVA due to its weak hydrogen bonding with polymer chains, whereas [EMIM] [ES] is highly hydrophilic (*36*). Upon immersion, [EMIM] [ES] rapidly infiltrates between the PVA molecular chains, disrupting PVA-water hydrogen bonds and displacing water into the surrounding IL phase. This solvent regulation effect drives PVA chains to aggregate and self-assemble via noncovalent crosslinks (hydrogen bonds and crystallites) (*35*). Simultaneously, the imidazole cations quickly combine with PVA hydroxyl groups, further promoting molecular association and network formation. This IL-mediated molecular reorganization rapidly converts a relatively thick PVA solution layer into a dense yet ultrathin polymer network while increasing the average intercrystalline spacing. In addition, the inherent hydrophilicity of [EMIM] [ES] allows the resulting ionogel to retain a small amount of water. This simple soaking process enables ultrafast ionogel formation within seconds, with film thickness readily controlled by the initial PVA coating thickness.

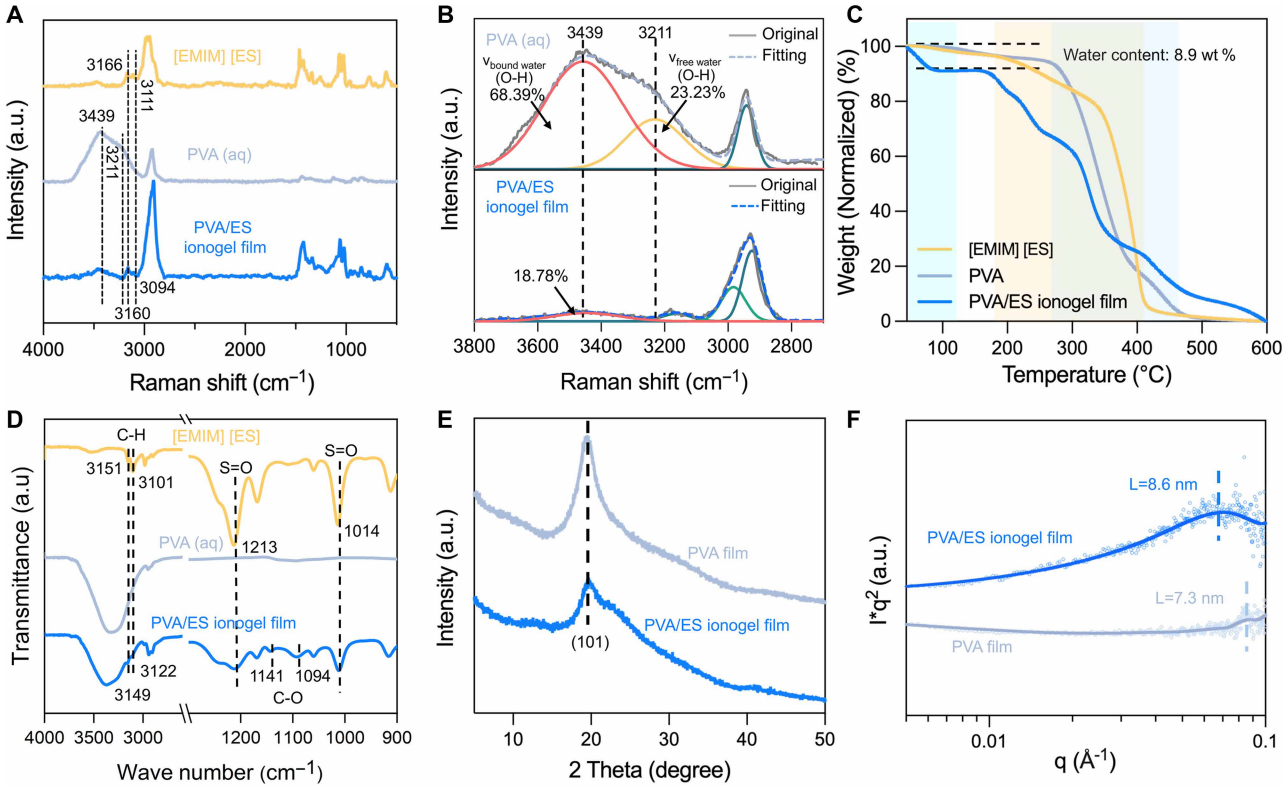

Fig. 2. Mechanism characterization and structural analysis of PVA/ES ionogel films. (**A** and **B**) Raman spectra of [EMIM] [ES], PVA aqueous solution (aq), and PVA/ES ionogel film (A) and corresponding fitting curves of PVA (aq) and PVA/ES ionogel film (B). (**C**) TGA curves of [EMIM] [ES], PVA, and PVA/ES ionogel film. (**D**) FTIR spectra of [EMIM] [ES], PVA (aq), and PVA/ES ionogel film. (**E** and **F**) XRD curves (E) and SAXS patterns (F) of PVA and PVA/ES ionogel films.

Comprehensive performance of PVA/ES ionogel films

A distinctive feature of the PVA/ES ionogel film is its high transparency, as demonstrated by the clear visibility of a green leaf vein beneath the film (inset of fig. S6). All ionogel films prepared with different IL induction times (5 s, 60 s, and 6 hours) exhibited transmittance values exceeding 80%, confirming excellent transparency (fig. S6). The multiple supramolecular crosslinking networks endow the PVA/ES ionogel film with outstanding mechanical robustness, which is a critical requirement for flexible electronic applications. As shown in Fig. 3A, the strip-shaped ionogel film could be stretched to more than five times its original length, showing good stretchability. Tensile tests were conducted to evaluate the mechanical properties of ionogel films prepared with different IL induction times (Fig. 3, B and C). After 5 s of IL induction, the ionogel film exhibited a tensile strength of 9.69 MPa, elongation at break of 552%, elastic modulus of 13.42 MPa, and toughness of 35.93 MJ m^{-3}. Prolonged IL induction resulted in progressive softening, characterized by decreased tensile strength and modulus but increased elongation. For instance, after 6 hours of IL induction, the ionogel film displayed an elongation of 675%, tensile strength of 6.78 MPa, and elastic modulus of 6.23 MPa. These mechanical variations primarily originate from the changes in water content and crystallinity. TGA revealed a gradual increase in both [EMIM] [ES] and water content with extended IL exposure, accompanied by a reduced PVA concentration (fig. S7), which was unfavorable for the formation of crystalline area (*34*). Raman spectra (fig. S8) corroborated the increase in water content, while FTIR analysis (fig. S9) showed diminishing intensities at 1141 and 1094 cm^{-1} with increasing induction time, indicating the weakened polymer-polymer interactions (*31*). XRD and differential scanning calorimetry (DSC) analyses further confirmed decreasing crystallinity: the diffraction peak at $2\theta = 19.6°$ (fig. S10) gradually diminished, and the crystallinity decreased from 8.65 to 7.92 wt % as the IL induction time increased from 5 s to 6 hours (fig. S11) (*38*). These results collectively confirm that the extended IL exposure diluted the PVA network and increased water and IL content, thereby reducing crystallinity and leading to the softening of the ionogel film. The mechanical properties of the ionogel film could also be tuned by adjusting PVA solution concentration (fig. S12). A concentration of 24% (w/v) produced a film that was excessively rigid, while 16% (w/v) resulted in poor film formation and insufficient strength. Thus, a 20% (w/v) PVA solution was identified as optimal for subsequent experiments. The mechanical toughness of the ionogel film was evaluated through pure shear tests, revealing a high fracture energy of ~22.6 kJ m^{-2} (fig. S13). Furthermore, the mechanical durability was assessed via cyclic tensile testing at 50% strain over 500 cycles (fig. S14). The ionogel film maintained structural integrity, with a large hysteresis loop in the first cycle (dissipated energy of 706 kJ m^{-3}; hysteresis ratio of 64.77%), indicating efficient energy dissipation via reversible hydrogen-bond fracture. From the 10th to 500th cycles, the hysteresis loop and ratio stabilized, suggesting enhanced structural stability after initial cyclic conditioning. These results confirm the good structural stability and durability of the ionogel film even when partial cross-linking points were broken, effectively preventing material failure caused by stress concentration during repetitive deformation

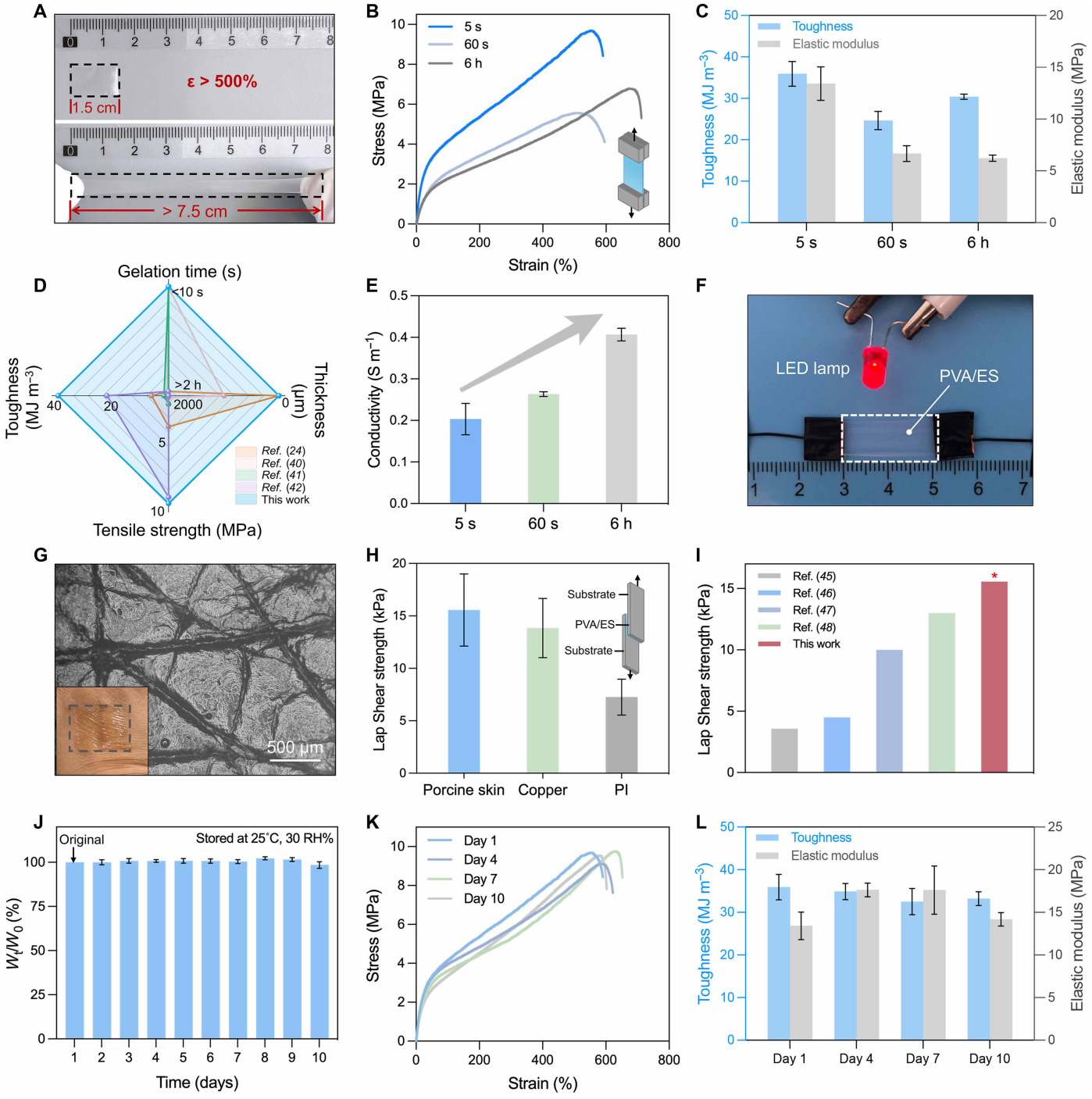

Fig. 3. Mechanical properties, conductivity, adhesion, and environmental stability of PVA/ES ionogel films. (**A**) Photographs showing the high stretchability of the PVA/ES ionogel film. (**B**) Tensile stress-strain curves and corresponding elastic modulus and toughness (**C**) of PVA/ES ionogel films fabricated with different induction times (5 s, 60 s, and 6 hours). (**D**) Radar chart comparing the PVA/ES ionogel film with previously reported ionic conductive gels in terms of gelation time, thickness, tensile strength, and toughness. (**E**) Conductivity of PVA/ES ionogel films as a function of induction time (5 s, 60 s, and 6 hours). (**F**) Photograph showing LED luminance using the PVA/ES ionogel film as conductors in series circuits. (**G**) Microscope and optical images of on-skin PVA/ES ionogel film peeled from skin. (**H**) Lap-shear strength of PVA/ES ionogel films to different substrates. The insert image shows schematic illustration of lap shear test. (**I**) Comparison of lap shear strength between the PVA/ES ionogel film and other gels used in bioelectronics. (**J**) Weight changes of the PVA/ES ionogel film at ambient conditions (25°C, 30% RH) for 10 days. (**K** and **L**) Tensile stress-strain curves (K) and corresponding elastic modulus and toughness (L) of the PVA/ES ionogel film stored under ambient conditions for different time periods. Error bars represent the SD of the measure values ($n = 3$).

(*39*). Our IL-induced self-assembly strategy enables rapid fabrication of ionogel films that combine ultrathin dimensions with high strength and toughness, outperforming previously reported ionically conductive gels (Fig. 3D) (*24*, *40*–*42*). Moreover, the ionogel film exhibited good ionic conductivity, reaching 0.2 S m^{-1} after only 5 s of IL induction and increasing with longer induction due to higher [EMIM] [ES] and water content (Fig. 3E). The conductive capability was visually demonstrated when an ionogel film completed an electric circuit to light an light-emitting diode (LED) (Fig. 3F). Notably, ionogel films with different thicknesses exhibited comparable tensile performance, fracture energy, and conductivity (figs. S15 and S16), validating the robustness of the fabrication process. Based on its rapid gelation, superior mechanical properties, and favorable ionic conductivity, the ultrathin PVA/ES ionogel fabricated with 5 s of IL induction was selected for further studies.

In practical applications as skin-mounted bioelectronics and flexible electronic substrates, robust adhesion is crucial for achieving stable, conformable attachment and minimizing interface impedance (*27*). The PVA/ES ionogel film exhibited conformal and robust adhesion to diverse substrates, facilitated by its ultrathin structure for intimate contact and abundant functional groups in PVA and ILs for strong interfacial interactions (*37*). Especially, because of rapid in situ gelation, the ionogel can be directly formed on complex surfaces (e.g., nonplanar, wrinkled, or hairy skin) within seconds, ensuring stable integration. For example, an in situ formed ionogel film on wrinkled skin remained firmly attached under repeated deformation (fig. S17 and movie S4). The optical microscopy of the detached ionogel film showed imprinted wrinkle patterns, confirming its excellent conformability to skin microstructures (Fig. 3G). The fluidic PVA solution also allowed seamless formation of ionogel films on hairy skin without interference (fig. S18). Adhesion was quantified by 180° peeling tests (fig. S19A). A uniform layer of PVA solution was deposited onto various substrates (e.g., porcine skin, copper, and PI), followed by overlaying with a second substrate and immersion in [EMIM] [ES] for 5 s to induce gelation. The two substrates were successfully adhered by the formed ionogel film. The calculated interfacial toughness values were 93.79, 56.22, and 14.67 J m^{-2} for porcine skin, copper, and PI, respectively (fig. S19, B and C). Lap shear tests (fig. S20) revealed adhesive strengths of 15.56 kPa on porcine skin, 13.84 kPa on copper, and 7.26 kPa on PI (Fig. 3H). The high adhesion strength to porcine skin can be attributed to abundant functional groups (e.g., hydroxyl and amine moieties) that facilitate hydrogen bonding interactions with the ionogel film (*43*). In addition, adhesion tests on ionogel films of varying thicknesses revealed that thinner films exhibited higher adhesive strength due to their lower flexural stiffness, which facilitates better conformal contact with the substrate (fig. S21), highlighting the great role of ultrathin structure in achieving strong adhesion (*44*). Compared with previously reported gel-based bioelectrodes (Fig. 3I and table S2), the PVA/ES ionogel film demonstrated superior adhesion performance, ensuring a stable skin-device interface essential for high-fidelity signal acquisition (*45*–*48*).

In addition, long-term environmental stability and tolerance to extreme conditions are critical for practical applications (*9*). Benefiting from the intrinsic stability of [EMIM] [ES], the PVA/ES ionogel film exhibited superior environmental tolerance. As shown in Fig. 3J, the ionogel film retained more than 95% of its initial weight after 10 days of storage at 30% relative humidity (RH) and 25°C. Tensile test revealed that the mechanical properties of the ionogel film remained almost unchanged throughout the storage period, with the ionogel film maintaining a tensile strain of 619%, tensile strength of 9.54 MPa, elastic modulus of 14.17 MPa, and toughness of 33.21 MJ m^{-3} after 10 days—more than 92% of the original values (Fig. 3, K and L). Meanwhile, the ionogel film preserved a high ionic conductivity of 0.2 S m^{-1} after 10 days (fig. S22). The ionogel film also remained stable across a wide range of humidity levels (30, 60, and 90% RH). Even under high humidity (90% RH), tensile strength and elongation retained 90 and 85% of initial values, respectively (fig. S23A), with ionic conductivity slightly increased due to additional water uptake (fig. S23B). In addition, the ionogel film exhibited excellent ultraviolet (UV) stability: Under continuous UV irradiation for 12 hours, transparency, mechanical performance, and ionic conductivity remained unaffected (fig. S24, A to C). Adhesion to porcine skin also remained stable after high humidity or UV exposure (fig. S25).

Furthermore, the mechanical robustness of the PVA/ES ionogel film was evaluated over a wide temperature range (fig. S26). Even after 10 days of storage at −40°C, the ionogel film remained high flexibility and could be stretched to 325% elongation despite exhibiting increased stiffness. Another critical property for wearable electronics is breathability, as poor moisture permeability can lead to skin irritation, inflammation, or occlusion during prolonged use (*17*). The ionogel film exhibited high water vapor transmission rate (WVTR), far surpassing that of commercial Ag/AgCl electrodes and PDMS film (fig. S27), approaching human sweat evaporation rates (600 g m^{-2} day^{-1}) (*49*), indicating excellent breathability and skin compatibility. As summarized in table S3, the ultrathin PVA/ES ionogel, with thickness as low as 13 μm and fabricated within merely 5 s, demonstrates a well-balanced combination of ultrahigh strength, good conductivity, robust interfacial adhesion, and excellent environmental stability, outperforming most previously reported ionic conductive gels. These multifunctional properties stem from the hydroxyl-rich PVA chains that facilitate robust noncovalent cross-linking, the IL-induced rapid self-assembly promoting the formation of crystalline domains, and the synergistic combination of IL and residual water, which collectively ensure efficient ionic transport and enhanced environmental durability. This fast-fabrication strategy holds great promise for next-generation skin-conformal, high-performance flexible electronics.

Painted PVA/ES ionogel bioelectrodes

Building on our strategy, we achieved direct fabrication of customized PVA/ES ionogels on human skin via rapid in situ gelation, akin to drawing temporary tattoos (fig. S28). By painting the PVA solution onto skin surface followed by immersion in [EMIM] [ES], we produced ultrathin, skin-conformal PVA/ES ionogel-based bioelectrodes (thickness: 39.3 ± 8.96 μm) with stable and robust skin-electrode interfaces for electrophysiological signal acquisition (fig. S29). The exceptional interfacial stability of these bioelectrodes arises from hydrogen bonding and ionic-dipole interactions between the painted ionogel film and skin constituents (Fig. 4A) (*6*). The ultrathin configuration minimizes interference with natural skin motion, ensuring imperceptible and comfortable wear. In contrast to commercial Ag/AgCl electrodes and thick PVA/ES ionogels (~0.6 mm), which induced skin impressions and erythema after 24 hours of wear, painted ultrathin ionogels adhered seamlessly on skin without causing redness or allergic reactions upon removal (fig. S30). To evaluate cutaneous biosafety, mouse skin contact experiments were conducted (*31*). Following the depilation of the dorsal region, the ionogel film

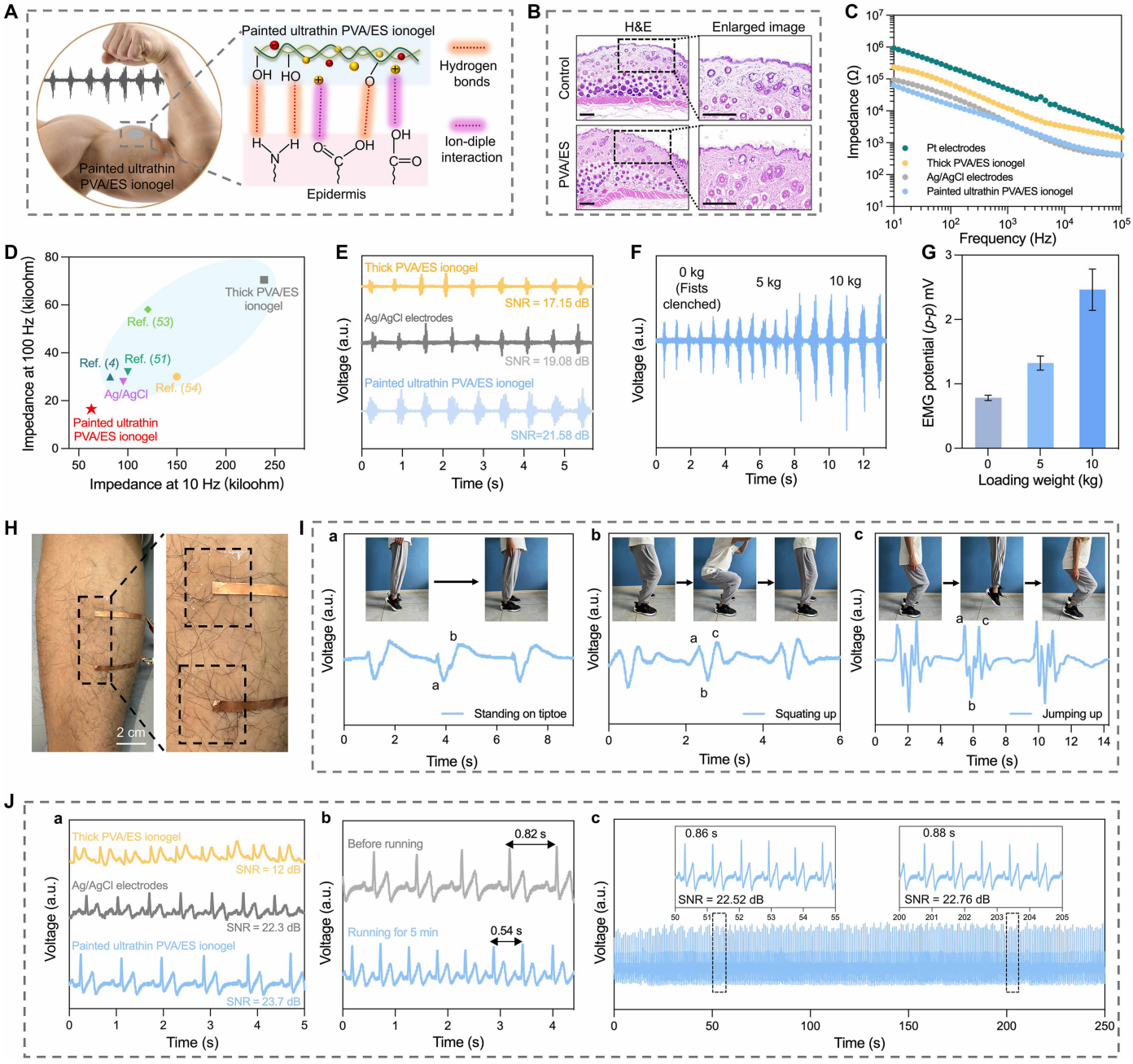

Fig. 4. Application of painted ultrathin PVA/ES ionogels as reliable bioelectrodes for recording electrophysiological signals. (**A**) Schematic illustration of the adhesion mechanisms of painted PVA/ES ionogel bioelectrodes on human skin. (**B**) H&E staining images of healthy tissue sections and tissue sections after 1 week of application with the PVA/ES ionogel film. Scale bar, 200 μm. (**C**) Skin interfacial impedance as a function of frequency for painted PVA/ES ionogel bioelectrodes, thick PVA/ES ionogels (~0.6 mm), commercial Ag/AgCl electrodes, and Pt electrodes. (**D**) Comparison of interfacial impedance at 10 and 100 Hz between painted PVA/ES ionogel bioelectrodes and other advanced gel-based bioelectrodes. (**E**) EMG signals captured by painted PVA/ES ionogel bioelectrodes, thick PVA/ES ionogels, and commercial Ag/AgCl electrodes. (**F** and **G**) EMG signals (F) and EMG potential (G) recorded during cyclic operation of a gripper under varying force levels. (**H**) Photographs depicting EMG testing conducted on hairy skin. (**I**) Detection of various body movements from EMG signals. The inset images illustrate typical actions: (a) standing on tiptoes, (b) squatting up, and (c) jumping. (**J**) ECG signals recorded by painted PVA/ES ionogel bioelectrodes, thick PVA/ES ionogels, and commercial Ag/AgCl electrodes (a). Comparison of ECG signals before and after running (b). Continuous ECG monitoring over 250 s using painted PVA/ES ionogel bioelectrodes (c). Error bars represent the SD of the measure values ($n = 3$). a.u., arbitrary unit.

was applied to the exposed skin and maintained for 7 days, after which the treated skin was sliced and stained with hematoxylin and eosin (H&E) for histological analysis. No noticeable inflammatory responses or structural abnormalities were observed in the epidermis or dermis compared to the control (Fig. 4B), confirming excellent skin biocompatibility. Owing to their robust skin conformity and good ionic conductivity, painted ultrathin ionogel bioelectrodes exhibited significantly lower interfacial impedance than thick PVA/ES ionogel, commercial Ag/AgCl, and Pt electrodes (Fig. 4C), favoring the acquirement of high-quality electrophysiological signals. This reduction is mainly attributed to the exceptional skin-conforming capability of the ultrathin ionogels (fig. S31). Unlike thick ionogels and conventional gel electrodes, which often failed to match microscale skin wrinkles, painted ultrathin ionogels formed a seamless, gap-free interface with the skin, thus minimizing interfacial impedance (*27*). The measured impedance values of our ultrathin PVA/ES ionogel bioelectrodes were 62.84 kΩ at 10 Hz [the primary frequency of electrocardiography (ECG)] and 16.59 kΩ at 100 Hz [the primary frequency of electromyography (EMG)], both markedly lower than those reported for existing gel-based bioelectrodes (Fig. 4D and table S4), highlighting the competitive advantage over existing advanced bioelectrodes (*4*, *18*, *41*, *50*–*56*).

Painted ultrathin PVA/ES ionogel bioelectrodes were applied to various skin sites for real-time EMG and ECG monitoring. For EMG recording, a pair of electrodes was positioned on the wrist flexor muscles to capture muscle activity (fig. S32). As shown in Fig. 4E, painted ionogel bioelectrodes reliably recorded EMG signals during continuous wrist flexor contractions, achieving a signal-to-noise ratio (SNR) of 21.58 dB—higher than those of thick PVA/ES ionogels (17.15 dB) and commercial Ag/AgCl electrodes (19.08 dB) (*57*). Painted ionogel bioelectrodes also demonstrated high sensitivity to varying gripping forces (0, 5, and 10 kg), with clear and distinguishable signal patterns (Fig. 4, F and G), suggesting potential in motor function assessment and rehabilitation monitoring. Benefiting from the conformal adhesion of in situ formed ultrathin PVA/ES ionogels, we further demonstrated their applicability on hair-covered skin regions by directly painting ionogel electrodes on the leg (Fig. 4H). EMG signals corresponding to different leg movements—including tiptoeing (a), squatting (b), and jumping (c)—were distinguishable (Fig. 4I). Tiptoeing generated two characteristic peaks, squatting yielded three peaks, and jumping produced three higher-amplitude peaks, enabling clear identification of muscle force generation. The exceptional mechanical robustness of painted ionogel bioelectrodes ensured stable skin adhesion during prolonged movements (e.g., tiptoeing), allowing accurate EMG recording during intense exercise, while low-toughness PVA/ES ionogel electrodes were prone to damage or detachment during motion, resulting in signal loss (fig. S33). These findings highlight the potential of painted ultrathin PVA/ES ionogel bioelectrodes for long-term neuromuscular monitoring, injury prevention, and real-time muscle fatigue evaluation.

For ECG monitoring, a dedicated setup was developed (fig. S34). As shown in Fig. 4J(a), painted ionogel bioelectrodes captured stable, high-quality ECG signals with resolved P-QRS-T waves and an SNR of 23.66 dB, outperforming thick PVA/ES ionogels (12 dB) and Ag/AgCl electrodes (22.3 dB). Heart rate after exercise increased from 73 to 111 beats per minute (bpm) [Fig. 4J(b)], demonstrating real-time physiological tracking. Continuous monitoring over 250 s showed consistent heart rate and SNR values between the early (50 to 55 s) and late stages (200 to 205 s) [Fig. 4J(c)]. The versatility of painted ionogel bioelectrodes was further confirmed by ECG monitoring during walking (83 bpm) and exercise (122 bpm), both of which showed well-defined P, QRS, and T waves with SNRs exceeding 18 dB (fig. S35A). In contrast, because of their limited ability to achieve a conformal interface with the skin surface, thick PVA/ES ionogels and commercial Ag/AgCl electrodes exhibited signal distortion and loss of ECG features during motions (fig. S35B). The above results demonstrate that painted ultrathin PVA/ES ionogels have great potential as high-performance bioelectrodes for sensitive and reliable EMG and ECG recording.

Customized flexible and stretchable integrated circuits and electrode arrays based on PVA/ES ionogel films

The ultrathin, transparent, stretchable, and mechanically robust PVA/ES ionogel film serves as an ideal substrate for printed stretchable electronics. Liquid metals (LMs), particularly gallium-indium alloys (EGaIn), are promising deformable conductors for applications in printed flexible circuits and high-density multichannel electrode arrays (*58*). However, their high surface tension and fluidity often limit compatibility with traditional substrates (*59*). Here, we formulated a conductive ink by blending EGaIn with PVA aqueous solution, which was then 3D printed onto the prepared PVA/ES ionogel film to fabricate flexible electronic devices (movie S5). The conductive ink was prepared by ultrasonically dispersing EGaIn into particles, followed by adding PVA solution under vigorous stirring (fig. S36). The hydroxyl groups of PVA formed hydrogen bonds with the oxide layer on EGaIn particles, improving dispersion uniformity and yielding a conductive ink well-suited for 3D printing. As illustrated in Fig. 5A, circuit interconnects were fabricated by directly printing EGaIn/PVA ink onto the ionogel film, followed by gentle rubbing to coalesce EGaIn particles and activate conductivity (fig. S37). The ultrathin ionogel film offers several advantages for stretchable circuit fabrication. First, the interfacial adhesion arising from unique water-activated hydroxyl groups on its surface facilitates strong bonding with the printed EGaIn/PVA layer via hydrogen bonding, ensuring robust circuit integration. Second, its ultrathin architecture allows conformal integration with nonplanar surfaces, which is critical for high–form factor electronic devices. Third, its excellent mechanical toughness provides structural stability and electrical reliability under large mechanical stresses. As shown in Fig. 5B, complex patterns and geometric shapes were successfully printed on the ionogel film using EGaIn/PVA conductive ink, with magnified images of spiral structures revealing high printing resolution. The well-integrated of EGaIn/PVA conductive ink on the ionogel film was confirmed by SEM images and the corresponding EDS elemental mapping (fig. S38). The customized circuits remained intact under substantial stretching and puncturing and adhered conformally to the skin, such as the back of a clenched hand without delamination (Fig. 5C, fig. S39, and movie S6), demonstrating the exceptional flexibility and skin compliance. In contrast, circuits printed on low-toughness ionogel films failed under large strain (fig. S40), while those on thicker ionogel films lacked conformability (fig. S41), limiting their ability to satisfy both mechanical and conformal requirements. Meanwhile, the ionogel film–EGaIn/PVA hybrid system exhibited excellent electrochemical stability with nearly unchanged cyclic voltammetry and electrochemical impedance spectroscopy curves after 1000 charge-discharge cycles (fig. S42). The consistent Nyquist profiles indicate negligible interfacial reactions between the LMs and ionogel matrix, confirming that the encapsulating

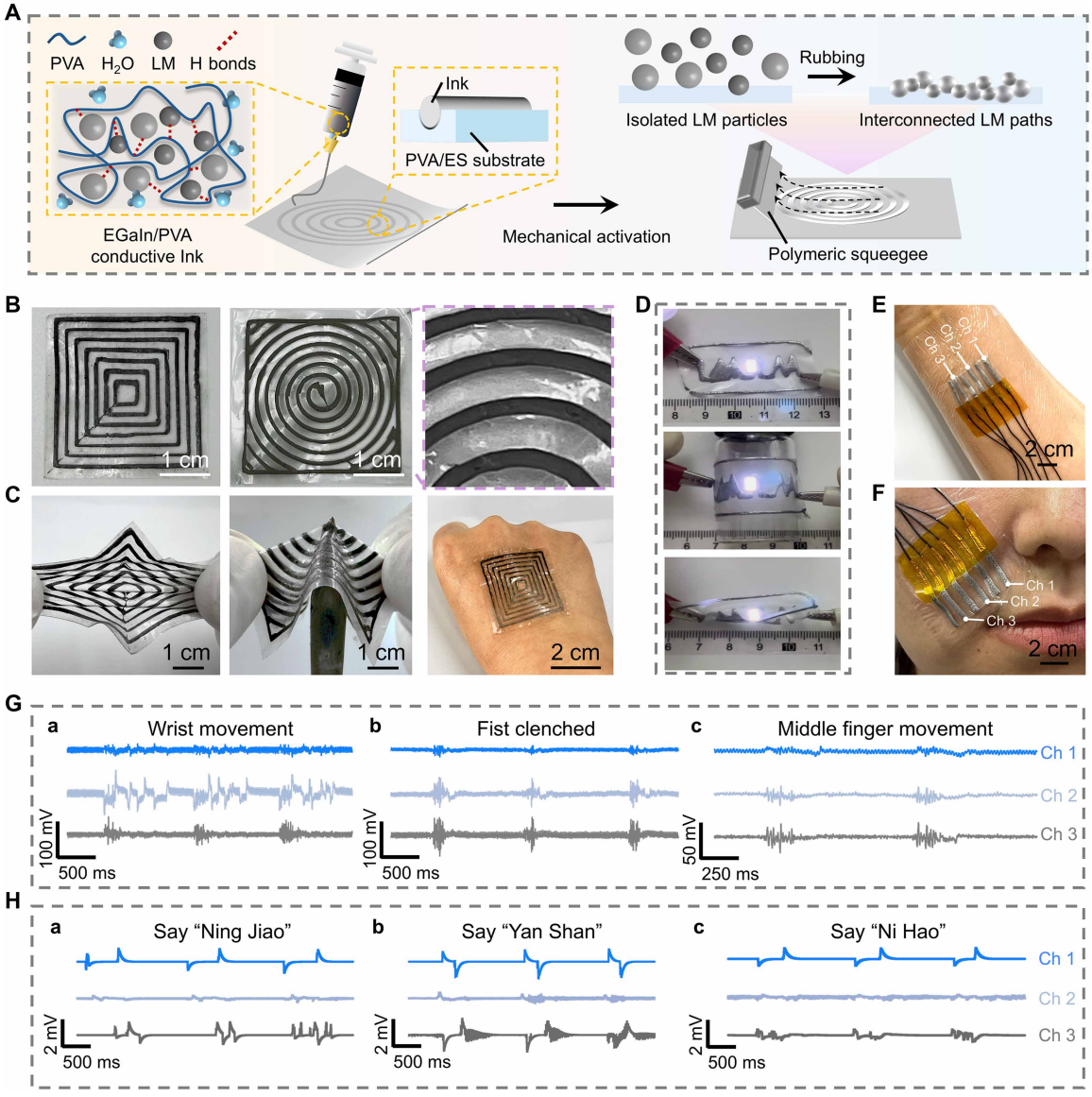

Fig. 5. Development of customized patterns on the PVA/ES ionogel film for flexible electronics. (**A**) Fabrication process of integrated circuits and electrode arrays including printing EGaIn/PVA ink on the PVA/ES ionogel film, followed by mechanical activation. (**B** and **C**) Photographs of printed EGaIn/PVA conductive ink circuits on the PVA/ES ionogel film demonstrating high printing resolution (B) and excellent robustness and conformability (C) including resistance to mechanical deformations such as stretching and puncturing, as well as seamless adhesion to the back of the hand. (**D**) Images of integrated circuits equiped with LED on the PVA/ES ionogel film under relaxing, laminating on a cylindrical surface, and twisting 180°. (**E** and **F**) Three-channel EGaIn/PVA/ES electrode patch positioned onto forearm muscle (E) and face (F) to dectect EMG signals. (**G** and **H**) Obtained three-channel EMG signals using the three-channel electrode array during three simple hand movements (G) and facial muscle movements during speaking (H).

PVA/ionogel network effectively suppresses EGaIn oxidation and ensures long-term electrochemical reliability. Furthermore, an ionogel film–based circuit incorporating a LED lamp was fabricated. When powered, the LED remained illuminated and functional under torsional deformation, maintaining electrical continuity (Fig. 5D and movie S7). A circuit with six LED patches interconnected via EGaIn/PVA tracks on the ionogel film also exhibited uniform brightness, demonstrating the ionogel film's potential as an effective interface for flexible electrode arrays (fig. S43).

Multi-channel bioelectronic arrays are pivotal for improving the spatial resolution and accuracy of physiological signal acquisition (*60*). Here, a three-channel EGaIn/PVA/ES electrode array was fabricated by directly printing EGaIn/PVA conductive ink onto the PVA/ES ionogel film. As illustrated in Fig. 5E, the electrode patch was conformally mounted onto the forearm to record EMG signals from muscle groups responsible for wrist flexion, extension, and finger articulation. Figure 5G demonstrates that the array could monitor and distinguish among three representative hand gestures: (a) wrist flexion followed by relaxation, (b) fist clenching and release, and (c) middle finger flexion and extension. Each motion produced distinct, reproducible EMG signals across the three channels, reflecting the temporal and spatial dynamics of muscle activation. The

analysis of the signal amplitude and waveform morphology enabled precise gesture classification. Beyond limb motion monitoring, the electrode patch also enabled reliable facial muscle tracking. As shown in Fig. 5F, the patch was attached to one side of the face to monitor facial muscle activity during speech. Different phrases—such as "Ning Jiao," "Yan Shan," and "Ni Hao"—produced diverse, reproducible EMG patterns (Fig. 5H), demonstrating the patch's capability to discern subtle facial movements associated with speech articulation. These results indicate that the three-channel EGaIn/PVA/ES electrode patch can accurately capture electrophysiological signals in both spatial and temporal dimensions, underscoring its potential for clinical applications such as neuromuscular disorder diagnosis.

Generality of IL-induced assembly for synthesizing ultrathin PVA ionogel films with adjustable mechanics

The ultrafast formation of the PVA ionogel films is driven by IL-induced cross-linking of PVA chains, which primarily rely on the effective contact between the IL and PVA aqueous solution, as well as the strong water affinity of the IL that disrupts PVA-water hydrogen bonds. This strategy is broadly applicable to ILs that are liquid at room temperature and have high hydrophilicity. To validate its generality, we prepared a series of PVA ionogel films using five additional ILs: EMIM trifluoromethanesulfonate (EMIM OTF), EMIM tetrafluoroborate (EMIM BF_4), 1-propyl-3-methylimidazolium tetrafluoroborate (PMIM BF_4), 1-butyl-3-methylimidazolium tetrafluoroborate (BMIM BF_4), and 1-butyl-3-methylpyridinium tetrafluoroborate (BMPY BF_4) (Fig. 6A). All these ILs enabled the rapid (<5 s) conversion of the PVA solution into ultrathin ionogels, which exhibited varying degrees of translucency depending on the IL used. We then systematically evaluated their mechanical performance (Fig. 6, B and C). The PVA ionogel films exhibited a wide range of toughness (35.93 to 183.36 MJ m^{-3}) and tensile strength (9.69 to 39.34 MPa), with all ionogel films showing remarkable stretchability (>400% strain; fig. S44). TGA analysis indicated that higher mechanical strength correlated with higher PVA content, following the order: BMIM BF_4 (54 wt %) < BMPY BF_4 (58 wt %) < PMIM BF_4 (68 wt %) < EMIM BF_4 (76 wt %) < EMIM OTF (80 wt %) (Fig. 6D and table S5). FTIR spectra (Fig. 6E) displayed a broad absorption band at 3000 to 3600 cm^{-1} in all ionogel films, assigned to the stretching vibration of hydroxyl groups ($\nu_{O\text{-}H}$) engaged in hydrogen bonding among PVA-PVA, PVA-water, and PVA-ILs. Peak-fitting analysis showed that the band at 3210 cm^{-1}, corresponding to PVA-PVA hydrogen bonding, accounted for a large proportion of the total area (fig. S45 and table S6), suggesting enhanced interchain interactions (*31*). XRD results confirmed a positive correlation between crystallinity and mechanical strength (Fig. 6F and fig. S46). Collectively, these results indicate that the tunable mechanical behavior originates from variations in IL-PVA compatibility: ILs with higher water affinity but weaker compatibility with PVA promote greater PVA chain aggregation and crystallization, thereby improving both mechanical robustness and opacity.

In summary, the mechanical properties of PVA ionogel films can be readily customized within a wide range by selecting ILs with different physicochemical characteristics. The achieved ultra-high toughness and fracture strength surpass that of most currently reported ionic gels and elastomers (Fig. 6G to I) (*9*, *22*, *61*–*71*). In addition, these ionogels demonstrated good ionic conductivity (fig. S47), and some also exhibited excellent skin compatibility (fig. S48), making them promising candidates for bioelectrode applications. Last, we demonstrated the facile printing of complex patterns using EGaIn/PVA ink on all these ionogel films (fig. S49), underscoring their potential as stretchable substrates for soft robotic skins, flexible displays, and other flexible electronic devices.

DISCUSSION

In summary, we have developed a facile and effective IL-induced self-assembly strategy for fabricating ultrathin PVA ionogel films. The introduction of IL [EMIM] [ES] into a high-viscosity PVA solution induced the rapid self-assembly of PVA chains, resulting in the formation of robust noncovalent cross-linking structures through both PVA-PVA and PVA-IL interactions. Ultrathin (13 to 103 μm) and large-area PVA/ES ionogels can be rapidly produced within seconds. The resulting ionogel films exhibited high strength (9.69 MPa), good stretchability (552%), remarkable toughness (35.93 MJ m^{-3}), favorable conductivity (0.2 S m^{-1}), as well as conformable adhesion and environmental stability. Moreover, this strategy enabled the rapid in situ formation of conformal and shape-adaptive ionogel coatings on a variety of irregular surfaces. These PVA/ES ionogels can be readily processed into on-skin bioelectronics with exceptional conformability and strong, durable contact with human skin, enabling high-fidelity acquisition of diverse electrophysiological signals (such as ECG and EMG). Furthermore, when used as a stretchable substrate, these ionogel films allowed the fabrication of integrated circuits and multichannel electrode arrays with high flexibility and reliability via 3D printing. The proposed strategy can be extended to different ILs, achieving rapid production of different PVA ionogel films with tunable mechanical properties. This work provides an effective method for the fast, in situ, and scalable fabrication of ultrathin ionogels with superior mechanical performance, holding great promise for applications in flexible electronics and related fields.

MATERIALS AND METHODS

Materials

PVA-1799 (98 to 99% hydrolyzed), EMIM BF_4, EMIM OTF, PMIM BF_4, BMIM BF_4 and ethanol were purchased from Shanghai Aladdin Bio-Chem Technology Co. Ltd. BMPY BF_4 was provided by Shanghai Macklin Bio-Chem Technology Co. Ltd. [EMIM] [ES] was purchased from Shanghai Leyan Reagents Company. EGaIn (gallium Indium eutectic, 99.99%) was provided by Sigma-Aldrich. Deionized water was used throughout the experiment. All the reagents were used as received.

Fabrication of PVA/ES ionogel film

First, the high-viscosity PVA solution was prepared by dissolving 2 g of PVA powers in 10 ml of deionized water under vigorous stirring at 95°C for 2 hours. After degassing, the homogeneous solution was uniformly coated onto a glass substrate via the doctor blade method. The freshly coated samples were immediately immersed in a sufficient amount of IL at room temperature. After soaking for 5 s, the resulting PVA/IL ionogel films were easily peeled from the glass surface. The PVA/ES films were optionally equilibrated at 25°C and 30% RH for 24 hours to ensure full stabilization. Various PVA ionogel films were obtained by varying IL species. Film thickness was controlled by adjusting the doctor blade height relative to the substrate.

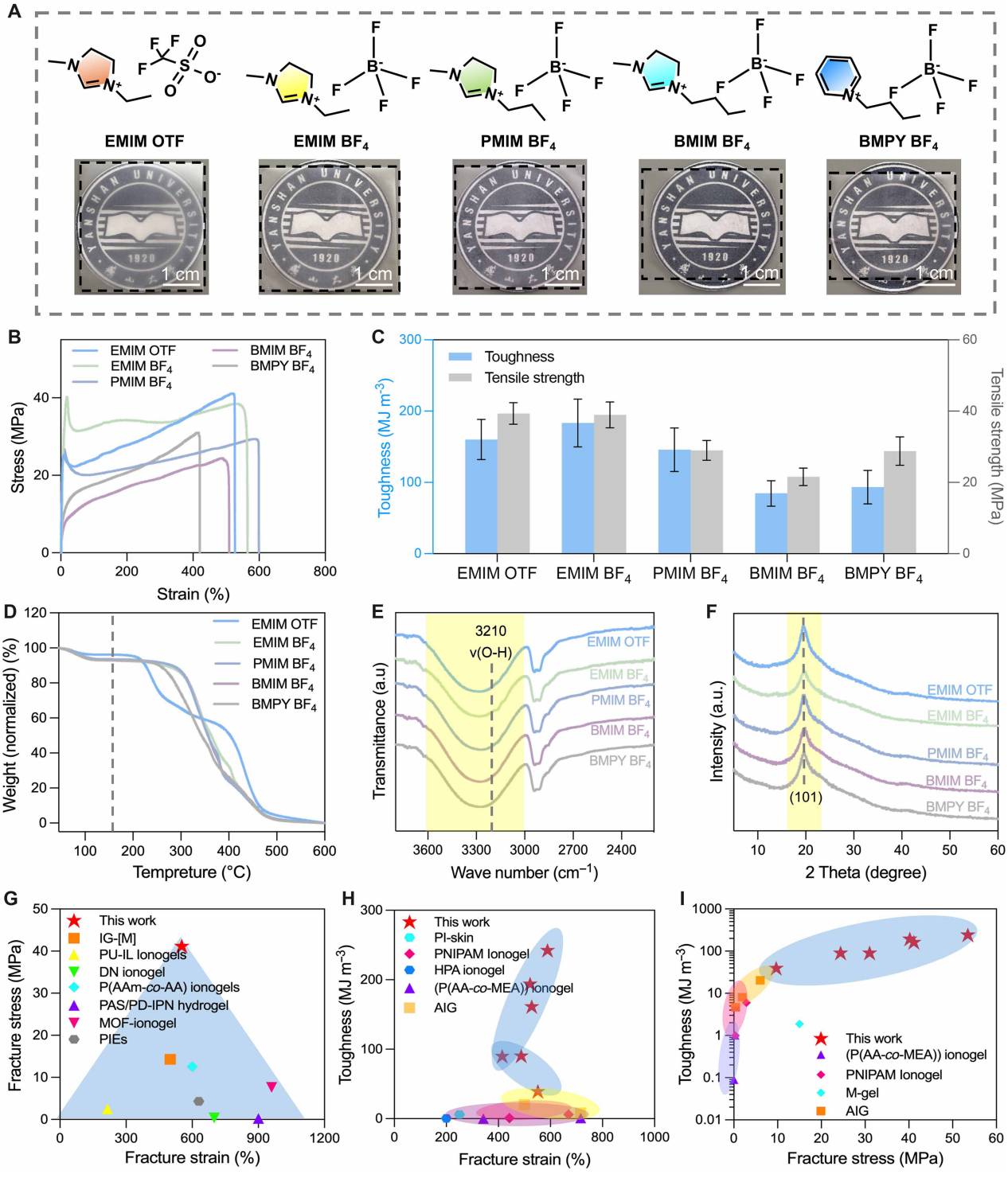

Fig. 6. Universality of the IL-induced assembly strategy for constructing various PVA ionogel films. (**A**) Chemical structures of different ILs and corresponding photographs of the obtained PVA ionogel films induced by these ILs. (**B** and **C**) Tensile stress-strain curves (B) and corresponding toughness and tensile strength (C) of different PVA ionogel films. (**D** to **F**) TGA curves (D), FTIR spectra (E), and XRD profiles (F) of various PVA ionogel films. (**G** to **I**) Ashby plots of fracture strain versus fracture stress (G), fracture strain versus toughness (H), and fracture stress versus toughness (I) of PVA ionogel films induced with different ILs and various representative composite ionic gels and elastomers reported in references. Error bars represent the SD of the measure values ($n = 3$).

Characterization

The chemical structures of the materials were analyzed by FTIR spectroscopy (Thermo Nicolet Corporation) in the range of 400 to 4000 cm^{-1} at room temperature. Spectral deconvolution was performed using Peak Fit software, with the 3000 to 3700 cm^{-1} region selected to ensure accurate baseline estimation. Raman spectra were obtained on a confocal Raman microscope (Horiba Jobin Yvon Xplora PLUS), and fitted within the 2700 to 3800 cm^{-1} range using the same software. XRD measurements was carried out on a Rigaku SMART LAB diffractometer with Cu-Kα radiation ($\lambda = 1.5418$ Å). SAXS was conducted on a Xeuss 2.0 system (Xenocs, France) at an x-ray wavelength of 1.54 Å, with a sample-to-detector distance of 2480 mm. The interdomain distance between adjacent crystalline domains (L) was calculated on the basis of Bragg's law ($L = 2\pi/q_{max}$, where q_{max} was the critical vector corresponding to the peak intensity). TGA was conducted by a TA Instruments Q50 system from 45° to 600°C at a heating rate of 10°C min^{-1} under N_2 atmosphere. DSC was performed on a Discovery DSC 250 (TA Instruments) under nitrogen flow. The crystallinity of samples was calculated as the ratio of the integrated melting peak area (210° to 260°C) from the DSC curve to the thermodynamic enthalpy of fusion for 100 wt % crystalline PVA (138.6 $J{\cdot}g^{-1}$). UV-visible transmittance spectra of various films were measured using a Shimadzu UV-2550 spectrophotometer in the range of 400 to 800 nm. A metallurgical microscope (LW3000) was used to observe the surface morphology of the painted PVA/ES film after being peeled from the skin and to measure the film thickness. SEM (SUPRA 55, Zeiss, Germany) was used to characterize the cross-sectional morphology of the PVA/ES film. In addition, EDS mapping was performed using the same instrument to analyze the elemental distribution within the film.

Mechanical test

The mechanical properties of PVA/ES ionogel films were assessed using a universal testing machine (Shimadzu AGS-X, Japan) equipped with a 100-N load cell at room temperature. Samples were cut into rectangular strips with dimensions of 30 mm by 5 mm, and film thickness was measured using a digital caliper. Unless otherwise stated, uniaxial tensile tests were conducted at a constant strain rate of 50 mm min^{-1}. Tensile strength and elongation at break were derived from the failure point on the stress-strain curves. The elastic modulus was calculated from the initial linear region of the stress-strain curve (0 to 5% strain), and toughness was defined as the area under the stress-strain curve up to failure. For cyclic tensile tests, films were repeatedly stretched to a predetermined strain and then released at the same rate without rest between cycles. The fracture toughness was evaluated by a pure shear test. Two identical rectangular samples with width of 5 mm and length of 20 mm (one with an initial notch width of 1 mm and one without notch) were subjected to monotonic tensile test in pairs. Both ends of each sample were clamped with an initial gauge length of ~10 mm and the strain rate was selected at 50 mm min^{-1}. The critical fracture strain was determined from the peak stress of the notched sample. The fracture energy (Γ) was calculated by the following equation

$$\Gamma = d\int_0^{\varepsilon} \sigma d\varepsilon$$

where, ε is the tensile fracture strain, σ is the tensile stress, and d represents the length of sample.

Conductivity test

Electrochemical workstation (CHI760E, CH Instruments, China) was used to test the conductivity of PVA/ES ionogel films by alternating current impedance method. The electrical conductivity was determined according to the formula

$$\sigma = \frac{L}{R \times S}$$

where L, R, and S represent the length (mm), resistance (ohm), and cross-sectional area (mm^2) of samples, respectively.

Adhesion test

A layer of PVA solution (50 mm by 10 mm by 0.1 mm) was applied between two same substrates (pigskin, copper, and PI), followed by immersion in IL for 5 s to form the films. Before the test, samples were equilibrated at 25°C and 30% RH for 24 hours. Actual contact dimensions were accurately measured using vernier calipers. The lap-shear and 180° peeling tests were used to evaluate the adhesive properties of the PVA/ES ionogel films. All tests were conducted at a speed of 50 mm min^{-1}. The adhesion strength was determined as the maximum load divided by the initial bonded area. The interfacial toughness was calculated by dividing twice the plateau force by the adhesion width.

Environmental stability analysis

To assess the environmental stability of the PVA/ES ionogel films, samples (30 mm by 30 mm) were stored at 25°C and 30% RH for 10 days. At designated time intervals, the weight of each sample was recorded, and the retained weight was calculated using the following equation

$$\text{Weight}\ (\%) = \frac{W_t - W_0}{W_0} \times 100$$

where W_0 represents the initial weight and and W_t denotes the weight at each time point during drying.

To assess the retention of functional performance, the mechanical properties and ionic conductivity of the ionogel films were measured after storage at 25°C and 30% RH for various durations. In addition, to investigate the influence of humidity, the films were conditioned at 25°C under different RH levels (30, 60, and 90%) for 24 hours, followed by evaluation of their tensile properties and conductivity. UV resistance was examined by exposing the PVA/ES ionogel films to continuous UV irradiation (Analytikjena UVL-28) for 12 hours, after which mechanical and electrical properties were tested. Furthermore, thermal stability was evaluated via uniaxial tensile tests at a series of temperatures (−40°, −25°, 25°, 40°, and 60°C).

Evaluation of gas permeability

Gas permeability was evaluated by measuring the WVTR. Glass bottles with an opening diameter of 11.54 mm were filled with 15 g of deionized water and sealed using the tested sample as a membrane. The sealed bottles were then placed in an environmental chamber maintained at 25°C and 30% RH. After 24 hours, the weight loss of each bottle was recorded, and the WVTR was calculated using the following equation

$$\text{WVTR} = \frac{m_{loss}}{S \times t}$$

where m_{loss}, t, and S are the water loss weight, time, and surface area, respectively.

Biocompatibility evaluation

The biocompatibility of the PVA/ES ionogel film was evaluated through rat skin attachment experiments. All experimental protocols were approved by the ethics committee of Yanshan University (approval no. 2022001). Male Sprague-Dawley rats (~6 weeks old, average body weight of ~180 g) were purchased from Beijing HFK Bioscience Co. Ltd. The rats were anesthetized, and a 40 mm–by–40 mm area of dorsal skin was depilated. Sterilized PVA/ES films (20 mm by 20 mm, UV-treated for 5 hours) were applied and secured with Tegaderm dressings for 7 days. Control rats underwent depilation only. On day 7, full-thickness skin tissues from both groups were harvested posteuthanasia, fixed in 10% formalin, stained with H&E, and examined via optical microscope (BX51, Olympus, Japan) for histological evaluation.

Electrophysiological signal acquirements

To evaluate the bioelectrical properties at the tissue-electrode interface, PVA/ES bioelectrodes were fabricated in situ on human skin. A square-shaped template (20 mm by 20 mm by 0.10 mm) was first attached to the skin surface. Subsequently, a PVA solution was applied onto the exposed area, followed by spraying [EMIM] [ES] (2 ml cm^{-2}) onto the liquid film, rapidly forming the PVA/ES bioelectrode. The EMG and ECG signals were recorded using a multichannel physiological signal acquisition system (RM6240XC, China). A healthy female volunteer aged 27 years participated in the study. To perform physiological signals detection experiments on human subjects, rules or permissions from the relevant national or local authorities are not in place in the country where the experiments were performed. The informed written consent of human participations was obtained before the experiments.

For EMG signal detection of the arm muscles, two PVA/ES bioelectrodes (20 mm by 20 mm) were fabricated on the brachioradialis muscle with an interelectrode distance of 4 cm. Measurements were conducted with a sensitivity of 1 mV, a low-pass filter cutoff frequency of 3 Hz, and a sampling rate of 1 kHz. Similarly, for leg EMG acquisition, two bioelectrodes of the same size and spacing were applied to the gastrocnemius muscle, with sensitivity set at 5 mV and identical filter and sampling parameters. For ECG monitoring, PVA/ES bioelectrodes were placed on the right arm, left arm, and left leg. The acquisition system was configured with a sensitivity of 0.2 mV, a 3-Hz low-pass filter, and a sampling rate of 800 Hz. For comparison, thick PVA/ES ionogel film and the commercial Ag/AgCl electrode were used. SNR was obtained from the formula

$$\mathrm{SNR\ (dB)} = 20 \times \log_{10}\left(\frac{V_{\mathrm{Signal}}}{V_{\mathrm{Noise}}}\right)$$

where V_{Signal} and V_{Noise} represent the peak-to-peak value of signal and noise, respectively.

Preparation of EGaIn/PVA inks

EGaIn (3 g) was mixed with 20 mL of anhydrous ethanol and sonicated for 1 hour in an ice bath using an ultrasonic cell disruption system to generate EGaIn particles. The resulting LM suspension was centrifuged at 8000 rpm for 10 min to obtain the sediment. Subsequently, 1 g of 10 wt % PVA solution was mixed with 3 g of EGaIn starch under stirring to form a uniform EGaIn/PVA dispersion. The EGaIn/PVA ink was stored in a sealed container to prevent evaporation.

Fabrication of flexible and stretchable electronics

A direct-ink-writing printer (AXO A3, Axolotl Biosystems Ltd., Austria) was used to fabricate flexible and stretchable electronics by printing EGaIn/PVA inks. Printing patterns were designed using AutoCAD software. The EGaIn/PVA inks were loaded into 3-ml syringes and extruded via pressure-driven flow. Nozzle diameters of 0.21 and 0.26 mm were selected according to design specifications, with extrusion pressures ranging from 10 to 30 kPa. After printing onto PVA/ES ionogel films, the devices were cured at 25°C for 12 hours, followed by mechanical activation to finalize the flexible electronics. LED patches were bonded onto the conductive tracks of the printed circuits using epoxy-based conductive silver (LX-50) and cured at room temperature for 24 hours to ensure stable electrical connections between the LEDs and the tracks.

Supplementary Materials

The PDF file includes:

Figs. S1 to S49
Tables S1 to S6
Legends for movies S1 to S7
References

Other Supplementary Material for this manuscript includes the following:

Movies S1 to S7

REFERENCES

1. Z. Zhang, W. Wang, Y. Jiang, Y.-X. Wang, Y. Wu, J.-C. Lai, S. Niu, C. Xu, C.-C. Shih, C. Wang, H. Yan, L. Galuska, N. Prine, H.-C. Wu, D. Zhong, G. Chen, N. Matsuhisa, Y. Zheng, Z. Yu, Y. Wang, R. Dauskardt, X. Gu, J. B.-H. Tok, Z. Bao, High-brightness all-polymer stretchable LED with charge-trapping dilution. *Nature* **603**, 624–630 (2022).
2. C. M. Tringides, N. Vachicouras, I. De Lázaro, H. Wang, A. Trouillet, B. R. Seo, A. Elosegui-Artola, F. Fallegger, Y. Shin, C. Casiraghi, K. Kostarelos, S. P. Lacour, D. J. Mooney, Viscoelastic surface electrode arrays to interface with viscoelastic tissues. *Nat. Nanotechnol.* **16**, 1019–1029 (2021).
3. S. Wang, J. Xu, W. Wang, G.-J. N. Wang, R. Rastak, F. Molina-Lopez, J. W. Chung, S. Niu, V. R. Feig, J. Lopez, T. Lei, S.-K. Kwon, Y. Kim, A. M. Foudeh, A. Ehrlich, A. Gasperini, Y. Yun, B. Murmann, J. B.-H. Tok, Z. Bao, Skin electronics from scalable fabrication of an intrinsically stretchable transistor array. *Nature* **555**, 83–88 (2018).
4. L. Zhang, K. S. Kumar, H. He, C. J. Cai, X. He, H. Gao, S. Yue, C. Li, R. C.-S. Seet, H. Ren, J. Ouyang, Fully organic compliant dry electrodes self-adhesive to skin for long-term motion-robust epidermal biopotential monitoring. *Nat. Commun.* **11**, 4683 (2020).
5. T. Li, H. Qi, C. Zhao, Z. Li, W. Zhou, G. Li, H. Zhuo, W. Zhai, Robust skin-integrated conductive biogel for high-fidelity detection under mechanical stress. *Nat. Commun.* **16**, 88 (2025).
6. L. Pan, P. Cai, L. Mei, Y. Cheng, Y. Zeng, M. Wang, T. Wang, Y. Jiang, B. Ji, D. Li, X. Chen, A compliant ionic adhesive electrode with ultralow bioelectronic impedance. *Adv. Mater.* **32**, 2003723 (2020).
7. Y. Jiang, K. Dong, X. Li, J. An, D. Wu, X. Peng, J. Yi, C. Ning, R. Cheng, P. Yu, Z. L. Wang, Stretchable, washable, and ultrathin triboelectric nanogenerators as skin-like highly sensitive self-powered haptic sensors. *Adv. Funct. Mater.* **31**, 2005584 (2021).
8. S. Jiang, B. Uch, S. Agarwal, A. Greiner, Ultralight, thermally insulating, compressible polyimide fiber assembled sponges. *ACS Appl. Mater. Interfaces* **9**, 32308–32315 (2017).
9. G. Ge, Y. Zhang, X. Xiao, Y. Gong, C. Liu, C. Lyu, W. L. Ong, G. W. Ho, Z. Yang, W. Huang, Rapidly gelling, highly adhesive, and mechanically robust ionogels for stretchable and wireless electronics. *Adv. Funct. Mater.* **34**, 2310963 (2024).
10. H. Qiao, S. Sun, P. Wu, Non-equilibrium-growing aesthetic ionic skin for fingertip-like strain-undisturbed tactile sensation and texture recognition. *Adv. Mater.* **35**, 2300593 (2023).
11. D. C. Kim, H. J. Shim, W. Lee, J. H. Koo, D.-H. Kim, Material-based approaches for the fabrication of stretchable electronics. *Adv. Mater.* **32**, 1902743 (2020).
12. W. Gao, J. Huang, J. He, R. Zhou, Z. Li, Z. Chen, Y. Zhang, C. Pan, Recent advances in ultrathin materials and their applications in e-skin. *InfoMat* **5**, e12426 (2023).
13. Q. Huang, Z. Zheng, Pathway to developing permeable electronics. *ACS Nano* **16**, 15537–15544 (2022).
14. W. Yeo, Y. Kim, J. Lee, A. Ameen, L. Shi, M. Li, S. Wang, R. Ma, S. H. Jin, Z. Kang, Y. Huang, J. A. Rogers, Multifunctional epidermal electronics printed directly onto the skin. *Adv. Mater.* **25**, 2773–2778 (2013).

15. C. Lim, Y. J. Hong, J. Jung, Y. Shin, S.-H. Sunwoo, S. Baik, O. K. Park, S. H. Choi, T. Hyeon, J. H. Kim, S. Lee, D.-H. Kim, Tissue-like skin-device interface for wearable bioelectronics by using ultrasoft, mass-permeable, and low-impedance hydrogels. *Sci. Adv.* **7**, eabd3716 (2021).
16. Y. Shin, H. S. Lee, Y. J. Hong, S.-H. Sunwoo, O. K. Park, S. H. Choi, D.-H. Kim, S. Lee, Low-impedance tissue-device interface using homogeneously conductive hydrogels chemically bonded to stretchable bioelectronics. *Sci. Adv.* **10**, eadi7724 (2024).
17. S. Cheng, Z. Lou, L. Zhang, H. Guo, Z. Wang, C. Guo, K. Fukuda, S. Ma, G. Wang, T. Someya, H. Cheng, X. Xu, Ultrathin hydrogel films toward breathable skin-integrated electronics. *Adv. Mater.* **35**, 2206793 (2023).
18. Z. Zhang, J. Yang, H. Wang, C. Wang, Y. Gu, Y. Xu, S. Lee, T. Yokota, H. Haick, T. Someya, Y. Wang, A 10-micrometer-thick nanomesh-reinforced gas-permeable hydrogel skin sensor for long-term electrophysiological monitoring. *Sci. Adv.* **10**, eadj5389 (2024).
19. Q. Gao, F. Sun, Y. Li, L. Li, M. Liu, S. Wang, Y. Wang, T. Li, L. Liu, S. Feng, X. Wang, S. Agarwal, T. Zhang, Biological tissue-inspired ultrasoft, ultrathin, and mechanically enhanced microfiber composite hydrogel for flexible bioelectronics. *Nano Micro Lett.* **15**, 139 (2023).
20. X. Fan, S. Liu, Z. Jia, J. J. Koh, J. C. C. Yeo, C.-G. Wang, N. E. Surat'man, X. J. Loh, J. Le Bideau, C. He, Z. Li, T.-P. Loh, Ionogels: Recent advances in design, material properties and emerging biomedical applications. *Chem. Soc. Rev.* **52**, 2497–2527 (2023).
21. J. Zhang, J. Yin, N. Li, H. Liu, Z. Wu, Y. Liu, T. Jiao, Z. Qin, Simultaneously enhancing the mechanical strength andIonic conductivity of stretchable ionogels enabled by PolymerizationInduced phase separation. *Macromolecules* **55**, 10950–10959 (2022).
22. M. Wang, P. Zhang, M. Shamsi, J. L. Thelen, W. Qian, V. K. Truong, J. Ma, J. Hu, M. D. Dickey, Tough and stretchable ionogels by in situ phase separation. *Nat. Mater.* **21**, 359–365 (2022).
23. Y. Zhu, Y. Guo, K. Cao, S. Zeng, G. Jiang, Y. Liu, W. Cheng, W. Bai, X. Weng, W. Chen, D. Zhao, H. Yu, G. Yu, A general strategy for synthesizing biomacromolecular ionogel membranes via solvent-induced self-assembly. *Nat. Synth.* **2**, 864–872 (2023).
24. J. Zhang, Z. Ma, M. Li, M. Lou, H. Wang, L. Jia, Development of ultrathin, breathable, waterproof, and durable nanonet-supported ionogel sensors for electrophysiological monitoring. *Adv. Funct. Mater.* **35**, 2415694 (2025).
25. J. Huang, J. Liu, X. Chen, J. Zhou, Y. Zhu, Q. Zhang, Ultrathin ionogels and hydrogels: Materials, mechanisms, and emerging applications. *J. Polym. Sci.* **63**, 3395–3409 (2025).
26. P. Xu, S. Challa, Z. Zhang, X. Wu, S. Wang, P. Pan, X. Liu, Ultrasoft, elastic, and ionically conductive polyethylene glycol/ionic liquid bottlebrush ionogels. *Mater. Horiz.* **12**, 7425–7438 (2025).
27. C. Wang, H. Wang, B. Wang, H. Miyata, Y. Wang, M. O. G. Nayeem, J. J. Kim, S. Lee, T. Yokota, H. Onodera, T. Someya, On-skin paintable biogel for long-term high-fidelity electroencephalogram recording. *Sci. Adv.* **8**, eabo1396 (2022).
28. M. Hua, S. Wu, Y. Ma, Y. Zhao, Z. Chen, I. Frenkel, J. Strzalka, H. Zhou, X. Zhu, X. He, Strong tough hydrogels via the synergy of freeze-casting and salting out. *Nature* **590**, 594–599 (2021).
29. J. Lv, G. Thangavel, Y. Xin, D. Gao, W. C. Poh, S. Chen, P. S. Lee, Printed sustainable elastomeric conductor for soft electronics. *Nat. Commun.* **14**, 7132 (2023).
30. J. Kiefer, J. Fries, A. Leipertz, Experimental vibrational study of imidazolium-based ionic liquids: Raman and infrared spectra of 1-ethyl-3methylimidazolium bis(trifluoromethylsulfonyl)imide and 1-ethyl-3-methylimidazolium ethylsulfate. *Appl. Spectrosc.* **61**, 1306–1311 (2007).
31. Y. Zhang, Y. Xiong, X. Li, S. Zhang, W. Xu, H. Chen, L. Xu, Oxidization and salting out synergistically induced highly elastic, conductive, and sensitive polyvinyl alcohol hydrogels. *Adv. Funct. Mater.* **35**, 2415207 (2024).
32. W. Ge, S. Cao, Y. Yang, O. J. Rojas, X. Wang, Nanocellulose/LiCl systems enable conductive and stretchable electrolyte hydrogels with tolerance to dehydration and extreme cold conditions. *Chem. Eng. J.* **408**, 127306 (2021).
33. H. Qiao, B. Wu, S. Sun, P. Wu, Entropy-driven design of highly impact-stiffening supramolecular polymer networks with salt-bridge hydrogen bonds. *J. Am. Chem. Soc.* **146**, 7533–7542 (2024).
34. X. Pan, J. Pan, X. Li, Z. Wang, Y. Ni, Q. Wang, Tough supramolecular hydrogels crafted via lignin-induced self-assembly. *Adv. Mater.* **36**, 2406671 (2024).
35. Y. Wu, Y. Zhang, H. Wu, J. Wen, S. Zhang, W. Xing, H. Zhang, H. Xue, J. Gao, Y. Mai, Solvent-exchange-assisted wet annealing: A new strategy for superstrong, tough, stretchable, and anti-fatigue hydrogels. *Adv. Mater.* **35**, 2210624 (2023).
36. L. Xu, S. Gao, Q. Guo, C. Wang, Y. Qiao, D. Qiu, A solvent-exchange strategy to regulate noncovalent interactions for strong and antiswelling hydrogels. *Adv. Mater.* **32**, 2004579 (2020).
37. H. Zhang, N. Tang, X. Yu, M.-H. Li, J. Hu, Strong and tough physical eutectogels regulated by the spatiotemporal expression of non-covalent interactions. *Adv. Funct. Mater.* **32**, 2206305 (2022).
38. X. Dong, X. Guo, Q. Liu, Y. Zhao, H. Qi, W. Zhai, Strong and tough conductive organo-hydrogels via freeze-casting assisted solution substitution. *Adv. Funct. Mater.* **32**, 2203610 (2022).
39. Z. Qin, Y. Li, X. Wang, Y. Liu, N. Li, Q. Xu, L. Ye, T. Jiao, High-strength, ultra-tough and recyclable MXene-composited organohydrogels with integrated multiple functions for wearable sensors. *J. Mater. Chem. A* **12**, 10808–10818 (2024).
40. D. Sun, Y. Feng, S. Sun, J. Yu, S. Jia, C. Dang, X. Hao, J. Yang, W. Ren, R. Sun, C. Shao, F. Peng, Transparent, self-adhesive, conductive organohydrogels with fast gelation from lignin-based self-catalytic system for extreme environment-resistant triboelectric nanogenerators. *Adv. Funct. Mater.* **32**, 2201335 (2022).
41. L. Li, X. Ye, Z. Ji, M. Zheng, S. Lin, M. Wang, J. Yang, P. Zhou, Z. Zhang, B. Wang, H. Wang, Y. Wang, Paintable, fast gelation, highly adhesive hydrogels for high-fidelity electrophysiological monitoring wirelessly. *Small* **21**, 2407996 (2024).
42. X. Wei, Z. Gou, J. Ye, L. H. Shi, J. Zhao, L. Yang, L. Zhang, K. Zhang, R. Jia, Stretchable full-color phosphorescent PVA-based ionogels for multimodal sensing-visual integration applications. *Adv. Sci.* **12**, 2411229 (2024).
43. F. B. Kadumudi, M. Hasany, M. K. Pierchala, M. Jahanshahi, N. Taebnia, M. Mehrali, C. F. Mitu, M. Shahbazi, T. Zsurzsan, A. Knott, T. L. Andresen, A. Dolatshahi-Pirouz, The manufacture of unbreakable bionics via multifunctional and self-healing silk–graphene hydrogels. *Adv. Mater.* **33**, 2100047 (2021).
44. F. Hannard, M. Mirkhalaf, A. Ameri, F. Barthelat, Segmentations in fins enable large morphing amplitudes combined with high flexural stiffness for fish-inspired robotic materials. *Sci. Robot.* **6**, eabf9710 (2021).
45. C. Cai, H. Zhu, Y. Chen, Y. Guo, Z. Yang, H. Li, H. Liu, Mechanoactive nanocomposite hydrogel to accelerate wound repair in movable parts. *ACS Nano* **16**, 20044–20056 (2022).
46. N. Li, X. Wang, Y. Liu, Y. Li, J. Li, Z. Qin, T. Jiao, Ultrastretchable, self-adhesive and conductive MXene nanocomposite hydrogel for body-surface temperature distinguishing and electrophysiological signal monitoring. *Chem. Eng. J.* **483**, 149303 (2024).
47. L. Wang, Z. Zhao, J. Dong, D. Li, W. Dong, H. Li, Y. Zhou, Q. Liu, B. Deng, Mussel-inspired multifunctional hydrogels with adhesive, self-healing, antioxidative, and antibacterial activity for wound healing. *ACS Appl. Mater. Interfaces* **15**, 16515–16525 (2023).
48. N. Li, Y. Li, Z. Cheng, Y. Liu, Y. Dai, S. Kang, S. Li, N. Shan, S. Wai, A. Ziaja, Y. Wang, J. Strzalka, W. Liu, C. Zhang, X. Gu, J. A. Hubbell, B. Tian, S. Wang, Bioadhesive polymer semiconductors and transistors for intimate biointerfaces. *Science* **381**, 686–693 (2023).
49. H. Yuk, T. Zhang, G. A. Parada, X. Liu, X. Zhao, Skin-inspired hydrogel–elastomer hybrids with robust interfaces and functional microstructures. *Nat. Commun.* **7**, 12028 (2016).
50. M. Xia, J. Liu, B. J. Kim, Y. Gao, Y. Zhou, Y. Zhang, D. Cao, S. Zhao, Y. Li, J. Ahn, Kirigami-structured, low-impedance, and skin-conformal electronics for long-term biopotential monitoring and human–machine interfaces. *Adv. Sci.* **11**, 2304871 (2023).
51. Y. Zhao, S. Zhang, T. Yu, Y. Zhang, G. Ye, H. Cui, C. He, W. Jiang, Y. Zhai, C. Lu, X. Gu, N. Liu, Ultra-conformal skin electrodes with synergistically enhanced conductivity for long-time and lowmotion artifact epidermal electrophysiology. *Nat. Commun.* **12**, 4880 (2021).
52. S. Pan, F. Zhang, P. Cai, M. Wang, K. He, Y. Luo, Z. Li, G. Chen, S. Ji, Z. Liu, X. J. Loh, X. Chen, Mechanically interlocked hydrogel–elastomer hybrids for on-skin electronics. *Adv. Funct. Mater.* **30**, 1909540 (2020).
53. H. Ye, B. Wu, S. Sun, P. Wu, Self-compliant ionic skin by leveraging hierarchical hydrogen bond association. *Nat. Commun.* **15**, 885 (2024).
54. X. Du, H. Wang, Y. Wang, Z. Cao, L. Yang, X. Shi, X. Zhang, C. He, X. Gu, N. Liu, An ultra-conductive and patternable 40 nm-thick polymer film for reliable emotion recognition. *Adv. Mater.* **36**, 2403411 (2024).
55. G. Ye, D. Song, J. Song, Y. Zhao, N. Liu, A fully biodegradable and biocompatible ionotronic skin for transient electronics. *Adv. Funct. Mater.* **33**, 2303990 (2023).
56. X. Shi, D. Song, W. Hu, C. Li, W. Zhang, S. Wang, Q. Hu, Y. Wang, X. Wang, Y. Zhang, B. Peng, Z. Wang, N. Liu, A sweat absorbing skin electrode for electrophysiology during exercise. *Adv. Funct. Mater.* **34**, 2314775 (2024).
57. W. Pei, H. Zhang, Y. Wang, X. Guo, X. Xing, Y. Huang, Y. Xie, X. Yang, H. Chen, Skin-potential variation insensitive dry electrodes for ECG recording. *IEEE Trans. Biomed. Eng.* **64**, 463–470 (2017).
58. M. A. Rahim, F. Centurion, J. Han, R. Abbasi, M. Mayyas, J. Sun, M. J. Christoe, D. Esrafilzadeh, F.-M. Allioux, M. B. Ghasemian, J. Yang, J. Tang, T. Daeneke, S. Mettu, J. Zhang, M. H. Uddin, R. Jalili, K. Kalantar-Zadeh, Polyphenol-induced adhesive liquid metal inks for substrate-independent direct pen writing. *Adv. Funct. Mater.* **31**, 2007336 (2021).
59. I. D. Joshipura, H. R. Ayers, C. Majidi, M. D. Dickey, Methods to pattern liquid metals. *J. Mater. Chem. C* **3**, 3834–3841 (2015).
60. S. Yang, J. Cheng, J. Shang, C. Hang, J. Qi, L. Zhong, Q. Rao, L. He, C. Liu, L. Ding, M. Zhang, S. Chakrabarty, X. Jiang, Stretchable surface electromyography electrode array patch for tendon location and muscle injury prevention. *Nat. Commun.* **14**, 6494 (2023).
61. X. He, Highly conductive and stretchable nanostructured ionogels for 3D printing capacitive sensors with superior performance. *Nat. Commun.* **15**, 6431 (2024).
62. X. Li, X. Yang, S. Li, H. Lv, Z. Wang, Z. Gao, H. Song, 3D printing of thermo-mechano-responsive photoluminescent noncovalent cross-linked ionogels with high-stretchability

and ultralow-hysteresis for wearable ionotronics and anti-counterfeiting. *Small* **20**, 2403252 (2024).
63. G. Jiang, G. Wang, Y. Zhu, W. Cheng, K. Cao, G. Xu, D. Zhao, H. Yu, A scalable bacterial cellulose ionogel for multisensory electronic skin. *Research* **2022**, 9814767 (2022).
64. Q. Xia, W. Li, X. Zou, S. Zheng, Z. Liu, L. Li, F. Yan, Metal–organic framework (MOF) facilitated highly stretchable and fatigue-resistant ionogels for recyclable sensors. *Mater. Horiz.* **9**, 2881–2892 (2022).
65. L. Li, W. Li, X. Wang, X. Zou, S. Zheng, Z. Liu, Q. Li, Q. Xia, F. Yan, Ultra-tough and recyclable ionogels constructed by coordinated supramolecular solvents. *Angew. Chem. Int. Ed.* **61**, e202212512 (2022).
66. T. Li, Y. Wang, S. Li, X. Liu, J. Sun, Mechanically robust, elastic, and healable ionogels for highly sensitive ultra-durable ionic skins. *Adv. Mater.* **32**, 2002706 (2020).
67. J. Sun, G. Lu, J. Zhou, Y. Yuan, X. Zhu, J. Nie, Robust physically linked double-network ionogel as a flexible bimodal sensor. *ACS Appl. Mater. Interfaces* **12**, 14272–14279 (2020).
68. X. Liu, X. Ji, R. Zhu, J. Gu, J. Liang, A microphase-separated design toward an all-round ionic hydrogel with discriminable and anti-disturbance multisensory functions. *Adv. Mater.* **36**, 2309508 (2024).
69. L. Peng, L. Hou, P. Wu, Synergetic lithium and hydrogen bonds endow liquid-free photonic ionic elastomer with mechanical robustness and electrical/optical dual-output. *Adv. Mater.* **35**, 2211342 (2023).
70. S. Xu, S. Wu, R. Zhu, Z. Qiu, Y. Yan, Fully physically crosslinked PNIPAM ionogels with high mechanical properties and temperature-managed adhesion achieved by H_2O/ionic liquid binary solvents. *Adv. Funct. Mater.* **34**, 2405965 (2024).
71. Y. Sun, X. Wang, H. Li, S. Zhang, W. Niu, Mechanically robust photonic-ionic skin cross-linked by metal–imidazole interactions. *Adv. Funct. Mater.* **34**, 2405345 (2024).
72. Y. Jiang, X. Zhang, W. Zhang, M. Wang, L. Yan, K. Wang, L. Han, X. Lu, Infant skin friendly adhesive hydrogel patch activated at body temperature for bioelectronics securing and diabetic wound healing. *ACS Nano* **16**, 8662–8676 (2022).
73. J. Luo, C. Sun, B. Chang, B. Zhang, K. Li, Y. Li, Q. Zhang, H. Wang, C. Hou, On-skin paintable water-resistant biohydrogel for wearable bioelectronics. *Adv. Funct. Mater.* **34**, 2400884 (2024).
74. W. Niu, Q. Tian, Z. Liu, X. Liu, Solvent-free and skin-like supramolecular ion-conductive elastomers with versatile processability for multifunctional ionic tattoos and on-skin bioelectronics. *Adv. Mater.* **35**, 2304157 (2023).
75. J. Xie, X. Li, Z. He, L. Fan, D. Yao, Y. Zheng, Preparation of tough and stiff ionogels via phase separation. *Mater. Horiz.* **11**, 238–250 (2024).
76. C. Luo, Y. Chen, Z. Huang, M. Fu, W. Ou, T. Huang, K. Yue, A fully self-healing and highly stretchable liquid-free ionic conductive elastomer for soft ionotronics. *Adv. Funct. Mater.* **33**, 2304486 (2023).
77. Q. Wang, S. Ling, X. Liang, H. Wang, H. Lu, Y. Zhang, Self-healable multifunctional electronic tattoos based on silk and graphene. *Adv. Funct. Mater.* **29**, 1808695 (2019).
78. Z. Yu, P. Wu, Water-resistant ionogel electrode with tailorable mechanical properties for aquatic ambulatory physiological signal monitoring. *Adv. Funct. Mater.* **31**, 2107226 (2021).
79. Z. Zhang, A. Yao, P. Raffa, Transparent, highly stretchable, self-healing, adhesive, freezing-tolerant, and swelling-resistant multifunctional hydrogels for underwater motion detection and information transmission. *Adv. Funct. Mater.* **34**, 2407529 (2024).
80. L. Xu, Z. Huang, Z. Deng, Z. Du, T. L. Sun, Z. Guo, K. Yue, A transparent, highly stretchable, solvent-resistant, recyclable multifunctional ionogel with underwater self-healing and adhesion for reliable strain sensors. *Adv. Mater.* **33**, 2105306 (2021).

Acknowledgments
Funding: Z.Q. and T.J. acknowledges the financial support from the National Natural Science Foundation of China (nos. 22102139 and 22372143), the Hebei Natural Science Foundation (nos. B2025203022 and B2025203050) and the Science Research Project of Hebei Education Department (No. JCZX2026028). **Author contributions:** Conceptualization: Z.Q., T.J., and X.H. Methodology: N.L., P.H., Y.Y., S.D., Y.L., X.S., Y.Q., and J.J. Investigation: N.L. and Z.Q. Visualization: N.L., P.H., and Z.Q. Supervision: Z.Q., T.J., and X.H. Writing—original draft: N.L., Z.Q., and X.H. Writing—review and editing: N.L., P.H., Z.Q., T.J., and X.H. **Competing interests:** The authors declare that they have no competing interests. **Data, code, and materials availability:** All data and code needed to evaluate and reproduce the results in the paper are present in the paper and/or the Supplementary Materials. Information on new materials is available in the Materials and Methods.

Submitted 13 August 2025
Accepted 21 January 2026
Published 27 February 2026
10.1126/sciadv.aeb4391

ScienceAdvances

Rapid self-assembly of robust ultrathin ionogel films for high-performance bioelectronics

Na Li, Ping He, Zhihui Qin, Yichen Yan, Sidi Duan, Yunfeng Li, Xiaojiao Shi, Yuxuan Qiao, Junan Jiang, Tifeng Jiao, and Ximin He

Sci. Adv. **12** (9), eaeb4391. DOI: 10.1126/sciadv.aeb4391

Science Advances (ISSN 2375-2548) is published by the American Association for the Advancement of Science. 1200 New York Avenue NW, Washington, DC 20005. The title *Science Advances* is a registered trademark of AAAS.